Thermal Rate Constant and Branching Ratio for CN + HD → HCN/DCN + D/H from T = 293 to 375 K

G. He, I. Tokue,† Lawrence B. Harding, and R. Glen Macdonald*

Argonne National Laboratory, Chemistry Division, 9700 South Cass Ave., Argonne, Illinois 60439

Received: May 27, 1998; In Final Form: August 3, 1998

The reaction rate constant for the cyano (CN) radical with deuterium hydride (HD) has been determined over the temperature range from 293 to 375 K. As well, the branching ratio for the partitioning into HCN + D or DCN + H has also been measured. The CN radical was detected by time-resolved near-infrared absorption spectroscopy using the CN ($A^2\Pi \leftarrow X^2\Sigma$) (2,0) band near 789.5 nm while the HCN molecule was monitored by time-resolved infrared absorption spectroscopy using the HCN(001) ← (000) υ_3 fundamental band near 3.0 μm. Both species were monitored following the same photolysis laser pulse used to generate the CN radical. The measurements were carried out in low pressures of Ar or He as carrier gas. The frequencies and structure of the transition states for all four isotopomers for CN + H_2 were calculated using ab initio quantum chemistry methods and a normal-mode analysis. Reasonable agreement was found between the experimental results and the rate constants predicted by conventional transition state theory using the theoretical transition state properties. These measurements should provide for an interesting test for theoretical predictions of thermal rate constants for this prototypical four-atom reaction system.

I. Introduction

The reaction of the cyano radical (CN) with H_2,

$$CN + H_2 \xrightarrow{k_{H_2}} HCN + H; \quad \Delta H_0 = -21.6 \text{ kcal mol}^{-1} \qquad \text{(RH2)}$$

has become an excellent candidate for detailed comparisons between theoretical predictions and experimental observations for a variety of properties relating to the kinetics and dynamics of this system. Much of this impetus has arisen from the recent development of a global potential energy surface (PES) by ter Horst et al.[1] These workers fit a large number of high-quality ab initio points based on a multireference configuration interaction (MR-CI) quantum chemistry calculation to describe the global interaction between CN and H_2, including the reactive HCN + H channel, and the various possible bound intermediate configurations, H_2CN and HNCH. This potential energy surface will be referred to as the TSH3 surface.

There have been a number of studies on the experimental determination of the thermal rate constant for reaction RH2 and its deuterated analogue

$$CN + D_2 \xrightarrow{k_{D_2}} DCN + D \qquad \text{(RD2)}$$

The early work has been summarized recently by Yang and Lin.[2] However, there was still some uncertainty as to the value of k_{H_2} near 300 K. Recent measurements, over a limited temperature range, from this laboratory[3] for k_{H_2} and k_{D_2} were in close agreement with measurements of Sun et al.,[4] Balla and Pasternack,[5] Juan and Smith,[6] and Sims and Smith.[7] New high-temperature shock tube measurements for k_{H_2} have also been reported by Wooldrige et al.[8] Over the past few years a great deal of dynamical information on the CN + H_2 reaction system has been obtained primarily by Liu and co-workers.[9−12] These workers have studied the deuterated analogue, reaction RD2, using crossed molecular beams and have determined the double differential cross sections, velocity- and angular-resolved, as a function of collision energy, almost at the vibrationally resolved level of detail. Che and Liu[10] measured the excitation function for reaction RD2 and found significant D atom product at collision energies ~1.0 kcal mol^{-1} below the barrier height derived from an earlier analysis of Wagner and Bair[13] and the best ab initio predictions of ter Horst et al.[1] Many of the findings determined by Che and Liu were in good agreement with theoretical predictions based on either full six-dimensional quasiclassical trajectory calculations[14] or reduced four-dimensional quantum calculations[15] using the TSH3 surface. Wang et al.[12] compared more refined differential cross-section measurements at a collision energy of 5.8 kcal mol^{-1} with full-dimensional quasiclassical trajectory calculations on the global TSH3 surface. Although the agreement between theory and experiment was good, these workers suggested that improvements in the PES, such as a lower barrier and tighter transition state, would make the agreement even better.

Other workers have looked at the HCN vibrational product state distribution from reaction RH2 by either infrared chemiluminescence[16] or time-resolved infrared absorption spectroscopy.[17] As deduced from the molecular beam experiments, considerable vibrational excitation in the HCN product was found in these experiments. Bethardy et al.[17] inferred that a large fraction of the initial HCN molecules were excited in the bending degree of freedom even though the transition state calculated by ab initio methods[1,13] was linear. Both full-dimensional quasiclassical trajectory calculations[14] and four-dimensional quantum calculations[15] for the HCN vibrational state distribution were in good agreement with the available experimental measurements.

† Department of Chemistry, Niigita University, Faculty of Science, Niigata 950-21, Japan.

S1089-5639(98)02391-3 CCC: $15.00
Published on Web 09/09/1998

Kinetic isotope effects have long been used to gain information on the shape of potential energy barriers for elementary chemical reactions involving the transfer of the light H atom. This was a primary motivation for the present experiments. The study of the reaction of $O(^3P)$ atoms with H_2, HD, and D_2 and the determination of the intramolecular kinetic isotopic branching ratio by Gordon and co-workers are prime examples of the usefulness of kinetic isotope effects in elucidating the features on a PES that may need to be adjusted to bring experiment and theory into better agreement.[18−20]

A reaction related to (RH2) is the reaction of $F(^2P)$ atoms with H_2. This reaction has played a central role in the field of chemical dynamics, and there have been numerous experimental and theoretical studies on this system. The intramolecular kinetic isotope effect has also been investigated for both thermal[21] and hot F atoms.[22] The rationalization of the observed preference for production of the HF product for thermal F atoms can be viewed from many different perspectives: transition state theory, information theory, kinematic effects, etc. A recent quasiclassical trajectory calculation, using a new high-quality ab initio PES,[23] looked at the intramolecular kinetic isotope effect in this system from a dynamical point of view.[24] Aoiz et al. addressed the differential cross section measurements of Neumark et al.[25] for the HF and DF channels, and as pointed out by Levine,[26] they found that the orientating nature of the PES played a major role in the dynamics. Thus, the rotational motion of the HD reactant greatly influenced the reactivity at the H end of the molecule.

Another four-atom system that has recently been studied experimentally is the $OH(^2\Pi) + H_2$ and its isotopomers. Talukdar et al.[27] measured the reaction rate constants, the kinetic isotope effect, and the intramolecular kinetic isotope effect as a function of temperature from 230 to 420 K. These workers used a variety of experimental techniques to probe the reactant and/or product OH/OD and product H/D atoms in real time. Interestingly, the measured rate constants for OH + HD were close to the average of the H_2 and D_2 isotopes; i.e., the OH abstracted an H atom independent of the isotopic nature of the uninvolved atom. These results were interpreted to imply that tunneling was the dominant reaction mechanism at the temperatures of the experiment.

In the present work, the thermal rate constant measurements for the CN + H_2 reaction system are further extended by measuring the thermal rate constant for the mixed isotope, HD, i.e.,

$$CN + HD \xrightarrow{k_{HD}} HCN/DCN + D/H \qquad \text{(RHD)}$$

and determining the branching ratio, Γ_{HCN} (or intramolecular kinetic isotope effect), defined here as the fraction of the total rate constant that produces HCN, i.e., $\Gamma_{HCN} = k_{HCN}/k_{HD}$, over the temperature range 293−375 K. The frequencies and structure of the saddle points for all four hydrogenic isotopomers were determined from a normal-mode analysis of the CN + H_2 transition state calculated at the multireference configuration interaction (MR-CI), complete active space (CAS) three-electron, three-orbital reference space level of theory. Using these properties for the transition states, k_{H_2}, k_{D_2}, k_{HD}, and Γ_{HCN} were calculated using conventional transition state theory (CTST) with Wigner tunneling.[28] The CTST rate constants were found to be in good agreement with the experimental measurements for all three isotopomers of H_2 if the barrier height was increased slightly to 4.2 kcal mol^{-1} from the ab initio value of 3.8 kcal mol^{-1}, calculated at the 3e-3o-CAS +1+2/pvtz level of theory.

TABLE 1: Mass Spectral Determination of the Composition of the HD Used in the Experiment

species[a]	vol %	species[a]	vol %
H_2	0.624± 0.062	N_2	<0.01[b]
HD	98.6 ± 0.3	C_2H_6	<0.007[b]
He	0.063 ± 0.006	O_2	<0.006[b]
D_2	0.621 ± 0.062	Ar	<0.007[b]
CH_4	<0.004[b]	CO_2	0.0025 ± 0.0020
H_2O	<0.05	C_3H_8	<0.01[b]
HDO	<0.05		

[a] No hydrocarbons greater than *m*/*z* of 44 noted on scan of entire gas. [b] Method detection limit.

The reaction was initiated by pulsed-laser photolysis of $(CN)_2$ to create the CN radical in a slowly flowing mixture of HD, inert gas, and $(CN)_2$. Both CN and HCN were detected by time-resolved absorption spectroscopy following the same photolysis laser pulse. The CN radical was detected using the (2,0) band of the red system $A^2\Pi \leftarrow X^2\Sigma$ electronic transition near 789.5 nm using a commercial, continuous wave, external cavity, diode laser. The utility of using this detection scheme for CN was suggested by Halpern and Huang several years ago.[29] The HCN molecule was detected using infrared absorption spectroscopy on the fundamental υ_3 band near 2.9 μm.

II. Experimental Section

The basic experimental apparatus has been described previously.[3,30] Briefly, the transverse flow reactor (TFR) consists of a stainless steel chamber that contains a Teflon box of dimensions 100 × 100 × 5 cm. The TFR was evacuated by a liquid nitrogen-trapped 25 cfm mechanical pump to an ultimate pressure of a few milliTorr. The leak rate of the TFR was less than 0.5 mTorr/min.

A separate, high-vacuum system was used to control the flow of gases into the TFR. The partial pressure of each component was determined from the known flow rate, as measured by calibrated electronic mass flow meters, and the total pressure. The H_2, He, and Ar gases were supplied by AGA gas and were all Research grade (99.9995% pure). The HD was supplied by Cambridge Isotopes Laboratory and certified to be better than 97% HD. The HD was independently analyzed by the Analytical Chemistry Laboratory at Argonne using a VG 3001 mass spectrometer. The chemical composition of the HD is given in Table 1 and was in excellent agreement with the supplier's specifications. The CN radical was generated by the 193 nm photolysis of $(CN)_2$ (Matheson Research grade, 98.5% pure). The photolysis laser was a Lumonics model 740 excimer laser, and the majority of experiments were carried out at a repetition rate of 5 Hz and power density of 2−10 mJ/cm.^{2}

The temperature of the TFR was varied over a modest range using a Nestlab model EX-251HT bath by circulating hot silicone oil through copper coils embedded in the top and bottom of the Teflon box. Part of the potential reaction zone was in sidearm chambers housing the White cell optics. The chambers were heated separately by heating tape to the same temperature as the TFR. The gas temperature was determined using five thermocouples, arranged as described previously.[3]

The CN reactant was detected using time-resolved absorption of the $^{12}C^{14}N(\upsilon=0)$ $R_1(8.5)$ line of the CN red system, $A^2\Pi \leftarrow X^2\Sigma$ (2,0) transition near 789.6 nm. The near-infrared laser was an Environmental Optical Sensors Inc. tunable, external cavity, diode laser. To ensure single-frequency operation, the diode laser output was continuously monitored using a 2 GHz free spectral range Etalon.

The HCN product was detected using time-resolved absorption of the υ_3 fundamental $H^{12}C^{14}N(000)$ P(8) transition near 3.05 μm. The tunable infrared laser was a single-mode Burleigh FCL-20 color center laser described previously.[30]

Both probe laser beams were overlapped and combined with the 193 nm photolysis laser beam using an UV−IR dichroic mirror mounted on the White cell optic axis near Brewster's angle for both horizontally polarized probe lasers. A ZnS optic, also set at Brewster's angle, was placed in front of the other White cell mirror to completely attenuate the 193 nm laser radiation. The White cell optical arrangement enabled both laser beams to pass directly through the photolysis zone 14 times for a path length of 14 m.

Two types of data were collected: time-resolved absorption traces to determine the kinetics of the CN + HD reaction system and frequency-resolved scans over absorption features of CN and HCN to determine the yield of HCN from the initial concentration of CN, $[CN]_0$, where the square brackets indicate concentration. The time-resolved absorption data for each species were recorded simultaneously by tuning the narrow-band laser radiation close to the peak of the appropriate absorption feature and signal averaging using both channels of a LeCroy 9410 digital oscilloscope. The lasers were then detuned several line widths, and background traces were recorded. Both signal plus background and background traces were transferred to a laboratory computer and subtracted to give the unperturbed absorption temporal profiles. The initial laser intensity, I_0, was either determined directly from the dc acquired trace or from a boxcar module, which sampled I_0 just before the photolysis laser was fired. The absorbance, $\ln(I_0/I)$, temporal profiles were calculated for further analysis. All the electronic amplifiers were set to dc so that at long decay times the traces would not be distorted by the truncation of low frequencies.[3]

The infrared laser could be manually tuned back and forth over an HCN absorption feature so that the frequency could be reliably positioned on the line center. On the other hand, the diode laser could only be scanned in one direction, and it was not possible to reliably determine the line center for the CN transition. To remove the uncertainty of tuning the laser frequencies to the peaks of the spectral lines, the peak absorption signals were determined by scanning the laser frequencies over each line at selected delay times following the initiating photolysis laser pulse. This required the use of four Stanford model 250 boxcar modules: two for each detected species, one to determine I_0 before the photolysis laser was fired, and one to record the signal, ΔI, at the preselected delay times. Each frequency-resolved scan was acquired in a point-by-point fashion by stepping either laser so that approximately 20 equally spaced frequency points defined a spectral line. The nominal shot-to-shot laser power from the excimer laser was also recorded, and the data were normalized for slight power variations of the excimer laser.

III. Results

A. Thermal Rate Constant Measurement. A complicating aspect of the measurements in this work was the presence of an unknown impurity in the vacuum system that gave rise to an HCN absorption signal in the absence of HD. There were two possible mechanisms for this HCN background; it could have been produced by direct reaction, CN + X → HCN + Y, or it could have been produced by photodissociation, X → HCN + Y. In either case, the mechanism for the background HCN production was important in order to account for its influence on the data analysis.

With no HD present, a flow of O_2 was added to the system while both CN and the impurity-generated HCN were monitored. The rapid reaction[31] of CN + O_2, $k = 2.5 \times 10^{-11}$ cm^3 molecule^{-1} s,$^{-1}$ removed the CN radicals with a simultaneous decrease in HCN. This experiment demonstrated that the HCN was not produced by direct photolyis but resulted from the reaction of CN with a background impurity. The impurity could have been introduced by one of the added gases; however, trap-to-trap vacuum distillations of the $(CN)_2$ from −85 to −196 °C and the use of different cylinders of the He or Ar carrier gases had no effect. It was concluded that the impurity was a contaminant of the vacuum system, and its influence was considered in the data analysis.

The following reaction sequence describes the reaction of CN with HD in the presence of an impurity X which produces HCN as a product:

$$(CN)_2 \xrightarrow{193\ \text{nm}} 2CN \quad (1)$$

$$CN + HD \xrightarrow{k_{HCN}} HCN + D \quad (2a)$$

$$CN + HD \xrightarrow{k_{DCN}} DCN + H \quad (2b)$$

$$CN + X \xrightarrow{k_X} HCN + Y \quad (3)$$

$$CN \xrightarrow{k_{diff}^{CN}} \quad (4)$$

$$HCN \xrightarrow{k_{diff}^{HCN}} \quad (5)$$

The kinetic equations describing this reaction sequence can be solved straightforwardly to give the time dependence of the CN and HCN concentrations, [CN(t)] and [HCN(t)], respectively:

$$[CN(t)] = [CN]_0 \exp(-k'_{CN}t) \quad (6)$$

$$[HCN(t)] = \frac{k_{HCN}[HD] + k_X[X]}{k'_{CN} - k_{diff}^{HCN}}[CN]_0\{e^{-k}diff^{HCN}{}_t - e^{-k'_{CN}t}\} \quad (7)$$

$$k'_{CN} = k_{HCN}[HD] + k_{DCN}[HD] + k_X[X] + k_{diff}^{HCN} \quad (8)$$

To a first-order approximation, because of their similar masses, the diffusion rates of CN and HCN should be similar in inert gases. Furthermore, the diffusion process has a complicated geometric dependence,[32] with four low-order diffusion modes described by two diffusion rate constants.[17] In the above reaction sequence the loss of CN and HCN by diffusion has been approximated by a single rate constant, and k_{diff}^{CN} will be assumed to be approximately equal to k_{diff}^{HCN}. In previous work from this laboratory, this has been shown to be a reasonable approximation, and the diffusion process can be considered to be a simple first-order process.[17] The k_{diff}^{HCN} was determined by monitoring HCN(000) for long times, after vibrational relaxation was complete, and fitting the absorbance profiles to a series of exponential terms, as described previously.[17]

Figure 1shows typical concentration profiles for HCN and CN when no HD was present. In Figure 1a the long time profile for HCN is shown. Note that the peak absorbance occurs almost 20 ms after the photolysis pulse and that the prelaser baseline is not quite flat, indicating that all the HCN produced in the previous laser pulse had not diffused from the photolysis zone,

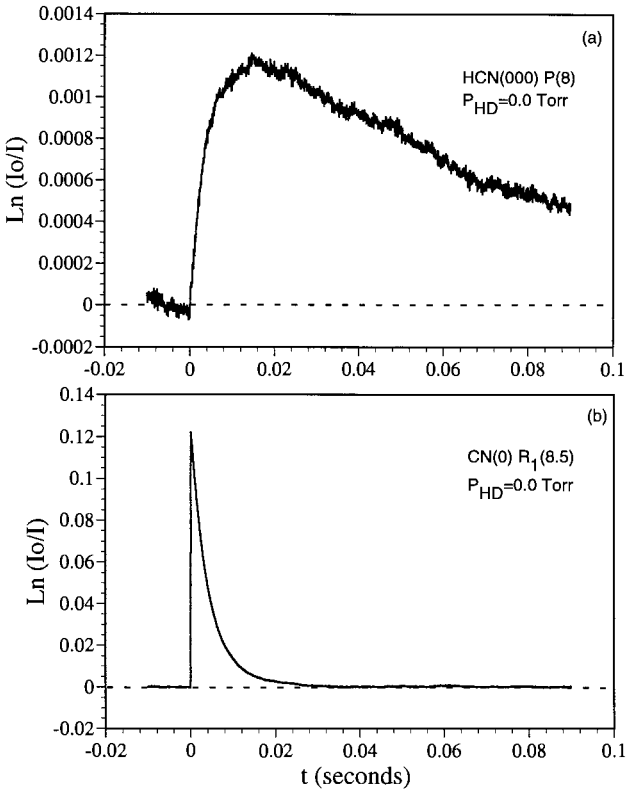

Figure 1. (a) Absorbance of background HCN(000) P(8) transition produced from CN reacting with an unidentified impurity in the TFR. The carrier gas was Ar with $P_{Ar} = 3.92$ Torr, and $P_{(CN)_2} = 0.005$ Torr and $T = 293$ K. The 193 nm photolysis laser had a nominal energy of 40 mJ/pulse and a repetition rate of 5 Hz. (b) Absorbance of CN(v=0) for the R_1(8.5) transition recorded simultaneously with the HCN absorbance trace shown in (a).

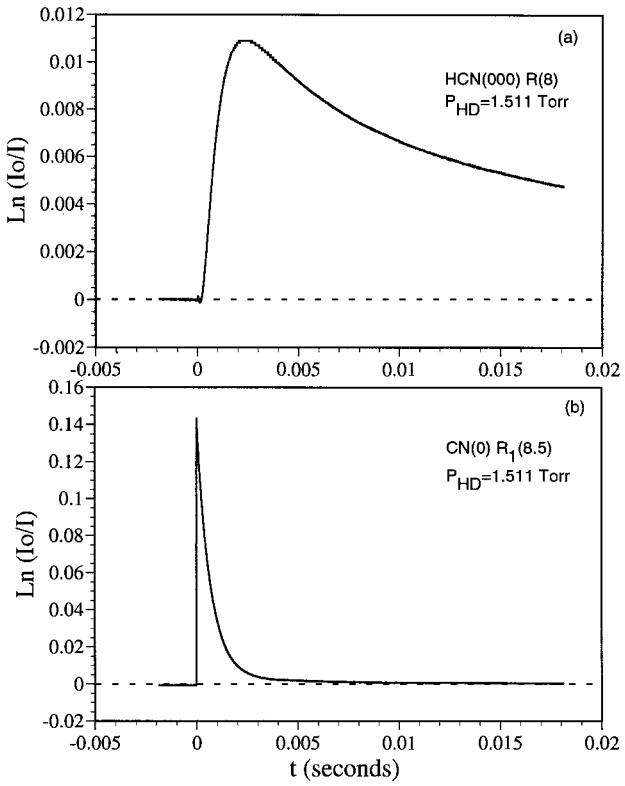

Figure 2. (a) Absorbance of HCN(000) P(8) for the same experimental run as in Figure 1, but with the $P_{HD} = 1.511$ Torr and the $P_{Ar} = 2.42$ Torr. The loss of HCN by diffusion is described by two exponential rate constants as discussed in the text. The HCN diffusion rate constants were determined to be 237 $^{-}$ and 31.6 $s.^{-1}$ (b) Absorbance of CN(0) R_1(8.5) for $P_{HD} = 1.511$ Torr simultaneously recorded with the HCN trace in (a). The single-exponential decay, k'_{CN}, was determined to be 1.28×10^3 s^{-1}.

even at the laser repetition rate of 5 Hz. However, the presence of the HCN background had no influence on the measurements of the reaction rate constant or branching ratio. At a photolysis laser repetition rate of 5 Hz, about 1% of the HCN remained in the photolysis region to be exposed to the next laser pulse. The absorption cross section of HCN at 193 nm is quite small, but even if completely photolyzed, the perturbation to the HCN probe laser intensity would be less than 0.01%. (Variation of the laser repetition rate from 1 to 10 Hz had no detectable influence on any measurements in the present work.) In Figure 1b the long time profile for CN(v=0) is shown, collected simultaneously with the HCN time profile in Figure 1a. Note that the CN profile reaches the prelaser baseline after 30 ms, indicating that the major loss channel for the CN radical is reaction with the background impurity, X. As well, the first-order decay of CN was larger than the faster diffusion rate constant for HCN in Figure 1a.

The procedure for determining the total reaction rate constant for CN with HD, $k_{HD} = k_{HCN} + k_{DCN}$, was the same as described previously.[3] Typical absorbance profiles for HCN and CN are shown in Figure 2, parts a and b, respectively. The absorbance profiles for CN and/or HCN were fit to single- and multiple-exponential functions using a nonlinear least-squares procedure. At a constant total pressure, the fast diffusion rate constant for HCN, k_{diff}^{HCN}, was determined and subtracted from the first-order decay rates for CN, k_{CN} (eq 8). The second-order rate constant, k_{HD}, was determined from the slope of $k_{CN} - k_{diff}^{HCN}$ plotted as a function of the partial pressure of HD, P_{HD}, at a constant total pressure of 4 Torr. The intercept of such a plot gave the contribution $k_X P_X$ (or k_X[X] as long as k_{diff}^{HCN} was approximately equal to k_{diff}^{CN}. Typical results of such an analysis are shown in Figure 3 for a total pressure of 3.9 Torr for the same experimental run from which Figures 1 and 2 were obtained. A summary of the data for the determination of k_{HD} as a function of temperature is presented in Table 2. Also included in the table are the values of the intercepts, $k_X P_X$, from the various runs.

B. Determination of the Branching Ratio, Γ_{HCN}. To determine Γ_{HCN}, the concentrations of both CN and HCN must be measured so that the amount of CN converted into HCN can be evaluated. This was accomplished by scanning over spectral lines of each molecule at known delay times following the photolysis laser pulse. Equations 6 and 7 described the time dependence of the [CN(t)] and the [HCN(t)] in the reaction system.

The measured absorbance, $A_B = \ln(I_0/I)$, of species B is related to the concentration of B by the Beer−Lambert law

$$\ln(I_0/I) = \sigma(\upsilon) l [\mathrm{B}] \tag{9}$$

where l is the path length and $\sigma(\upsilon)$ is the absorption cross section at frequency υ. If the frequency distribution of the radiation source is much narrower than the absorption feature, then $\sigma(\upsilon)$ is related to the line strength of the transition, S_{ji}, by

$$\sigma(\upsilon) = S_{ji} g(\upsilon) \tag{10}$$

where $g(\upsilon)$ is the line shape function, either a thermal Doppler profile or Voigt profile for the low pressures used in the present experiments. The line strength is the fundamental quantity for

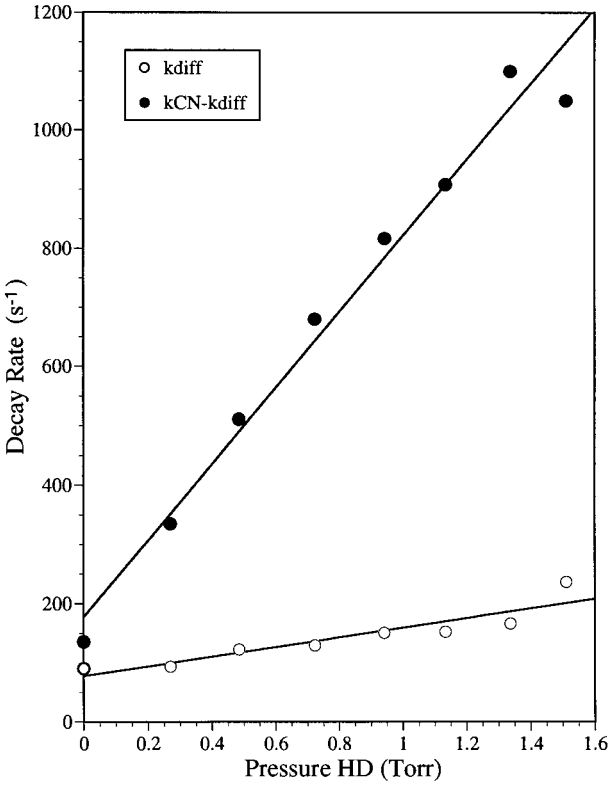

Figure 3. First-order rate constants (●) plotted as a function of P_{HD} for the experimental run in which Figures 1 and 2 were recorded. The diffusion rate constant for CN (○) was taken from the larger decay rate of HCN and subtracted from k'_{CN}. The slope of $k'_{CN} - k_{diff}$ vs P_{HD} gives k_{HD} and the intercept $k_X P_X$. The least-squares estimates for these parameters were $k_{HD} = 642 \pm 41$ Torr^{-1} s^{-1} and $k_X P_X = 178 \pm 38$ s^{-1}, where the uncertainty is ± 1 standard deviation.

TABLE 2: Summary of the Data for the Determination of k_{HD} as a Function of T[a]

T (K)	carrier gas	P_{total} (Torr)	$k_{HD} \times 10^{14}$ (cm^3 molecule^{-1} s^{-1})	$\pm\sigma$	$k_X P_X$ (s^{-1})	$\pm\sigma$
293	Ar	2.0	1.88	0.16	271	40
293	Ar	4.0	1.96	0.12	178	38
293	He	4.0	2.15	0.21	250	47
301	He	4.0	2.05	0.13	330	42
318	He	4.0	2.58	0.18	351	67
320	He	4.0	2.86	0.20	372	26
340	He	4.0	4.54	0.11	400	12
362	He	4.0	6.23	0.55	735	65
367	He	4.0	6.15	0.72	725	192
367	He	4.0	5.94	0.27	306	121
374	He	4.0	7.46	0.43	670	38
375	He	4.0	7.50	0.79	703	79

[a] The uncertainties ($\pm\sigma$) are the standard error values returned in the least-squares fitting of the data.

the probed spectroscopic transition and is directly related to the transition moment. The infrared vibrational transition moment for the v_3 HCN(001) ← (000) transition has been accurately measured in several laboratories.[33,34] For CN, the situation is not so straightforward because of the transient nature of the CN radical. Currently, the best estimate of the electronic−vibrational transition moment for the CN red system comes from high-quality ab initio calculations.[35] In the course of the present experiments, the electronic−vibrational transition moment for the (2,0) band of the CN red system was measured and found to be in good agreement with the theoretical predictions. The details of these experiments will be given elsewhere.[36] As will be shown in the following, only the ratio of the peak absorption coefficients, given by a calibration factor, cal = $\sigma_{CN}(v_0)/\sigma_{HCN}(v_0)$, where v_0 is the peak frequency of the probed transition, was needed for the determination of Γ_{HCN}. The calibration factor was evaluated under identical conditions but in separate experiments on the CN + H_2 reaction, for which there is a direct correspondence between the initial CN concentration and the final HCN concentration. The use of the calibration factor accounted for the production of CN(v=1) in the photolysis of $(CN)_2$. The calibration factor was found to be 5.9 ± 0.8, independent of temperature, within the scatter of the data, because of the similarity of rotational constants for CN and HCN and the limited temperature range of the measurements.

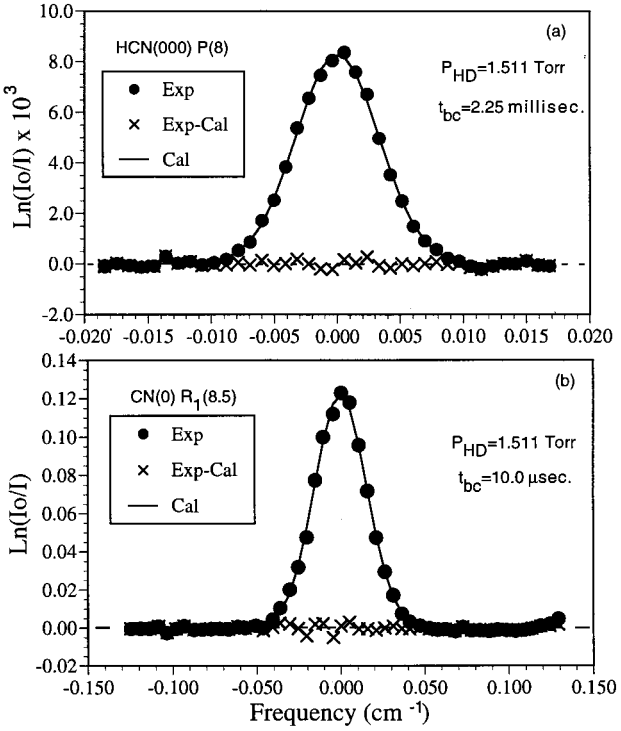

Figure 4. (a) Scan over the HCN(000) P(8) absorption feature for the same experimental run as in Figures 1 and 2. The profile was recorded with $t_{bc}^{HCN} = 2.25$ ms at the peak of the temporal absorbance profile in Figure 2a. The solid line is a nonlinear least-squares fit to a Gaussian profile with a fwhm width of 0.007 89 cm.$^{-1}$ The ×'s are the difference of the fit from the experimental points. (b) Same as in (a) except a scan over the CN(0) R_1(8.5) absorption line collected simultaneously with the HCN(000) P(8) profile in (a). In (b), $t_{bc}^{CN} = 10$ μs, and the fwhm width was 0.0305 cm^{-1}.

The experiment probed state-specific populations so that care must be taken to ensure that the frequency-scanned measurements were representative of the total population for each molecule. To monitor CN, the $^{12}C^{14}N$(0) R_1(8.5) transition was probed at a delay time, t_{bc}^{CN}, of 5−10 μs, and for HCN, the $H^{12}C^{14}N$(000) P(8) transition was probed at a delay time, t_{bc}^{HCN}, of 1−3 ms, depending on the reaction time scale.

Typical scans over the absorption lines for HCN(000) P(8) and CN(0) R_1(8.5), recorded under the same experimental conditions as the temporal absorbance profiles shown in Figure 2, are presented in Figure 4. The single-line absorption profiles were fit to a Gaussian form using a nonlinear least-squares fitting procedure based on Marquardt's method.[37] As is evident, the spectral lines were well-described by a Gaussian line shape with a width nearly equal to the expected Doppler value.

The frequency-scanned measurements, recorded at different times for CN and HCN, were related to each other using the following procedure to give an expression involving k_{HCN}[HD].

The initial concentration of CN, $[CN]_0$, can be eliminated from eq 7 using eq 6 to give

$$\frac{[HCN(t_{bc}^{HCN})]}{[CN(t_{bc}^{CN})]}\frac{(k'_{CN}-k_{diff}^{HCN})}{e^{k'_{CN}t_{bc}^{CN}}\{e^{-k_{diff}^{HCN}t_{bc}^{HCN}}-e^{k'_{CN}t_{bc}^{HCN}}\}}=k_{HCN}[HD]+k_X[X] \quad (11)$$

The peak absorbances for HCN and CN, $A_{HCN}(t_{bc}^{HCN})$ and $A_{CN}(t_{bc}^{CN})$, as shown in Figure 4, were used to determine the ratio $[HCN(t_{bc}^{HCN})]/[CN(t_{bc}^{CN})]$ according to eq 9 as

$$\frac{[HCN(t_{bc}^{HCN})]}{[CN(t_{bc}^{CN})]}=\frac{A_{HCN}(t_{bc}^{HCN})}{A_{CN}(t_{bc}^{CN})}\frac{\sigma_{CN}(\nu_0)}{\sigma_{HCN}(\nu_0)} \quad (12)$$

Only the ratio of effective absorption cross sections given by the calibration factor, cal, was needed in the data analysis. All the rate constants used to evaluate eq 11 were determined in the same experimental run, including the determination of the $k_X[X]$.

Two methods were used to evaluate the $k_X[X]$ term in eq 11. The most reliable was to use the intercept provide by plotting $k'_{CN} - k_{diff}^{HCN}$ as a function of P_{HD}, as shown in Figure 3. The second procedure was to use the background generated temporal absorbance profile of HCN, i.e., for $P_{HD} = 0.0$, combined with scans over the CN and HCN absorption features with no HD reactant in the system and to evaluate the $k_X[X]$ term according to eq 11. Generally, these two measurements were within ±30% of each other. The determination of the $k_X[X]$ term from the background absorption signals was considered the least reliable because of the long delay time at which the measurement of the background [HCN] was made. To further reduce the influence of the background reaction on the results, data for which the $k_{HCN}[HD]$ term was less than $2k_X[X]$, i.e., $P_{HD} <$ 0.8 Torr, were not considered in the reported results.

The determination of the branching ratio, Γ_{HCN}, was made by subtracting the measured value for the $k_X[X]$ term from the left-hand side of eq 11 and dividing the calculated value of k_{HCN}-[HD] by the value of $k_{HD}[HD]$ obtained in the time-resolved experiments under the same conditions as the frequency-resolved measurements.

The simultaneous scanning of the CN reactant and HCN product absorption features on each photolysis laser pulse minimized the experimental uncertainty that would occur in the normalization of separate experiments to monitor each species and removed any uncertainty in tuning the laser frequencies to the appropriate line centers. The data for the experimental measurements for the Γ_{HCN} as a function of temperature are shown in Figure 5along with the calculated value based on CTST that will be discussed later.

The absolute error bars for the determination of $\Gamma_{HCN} = k_{HCN}/k_{HD}$ are considerably larger than those due to experimental scatter alone. It was estimated that the absolute uncertainty was ±15%, resulting from the uncertainty in the calibration factor in relating the peak absorption cross section for CN to that for HCN and the uncertainty in the determination of k_{HD}. To circumvent some of these difficulties, the data were analyzed with all the parameters determined from a single experimental run. This procedure should suppress some systematic variations from run to run and produce more reliable results.

C. Influence of Excess Rotational and Vibrational Energy in CN and HCN. As already noted, measurements were made on only a single quantum state of each species so that the effects of internal excitation should be considered. The largest influence on the determination of Γ_{HCN} would likely arise from vibrationally excited CN radicals. The photolysis of $(CN)_2$ at 193 nm produces 13% of the initial CN radicals in CN(v=1).[38] The tuning range of the diode laser was not sufficient to reach the spectral region for the CN $A^2\Pi \leftarrow X^2\Sigma^+$ (3−1) band so that the [CN(v=1)] could not be monitored. Vibrationally excited CN could influence the experimental results in two ways, through reaction and vibrational relaxation; however, both effects were expected to be small. The loss of CN(v=1) with H_2 and D_2 has been investigated by several workers and has been attributed to reaction with only a slightly larger rate constant than for CN(v=0).[7,39] As well, theoretical predictions for the thermal rate constant for CN(v=1) + H_2, based on the TSH3 surface, show that the reactivity of CN(v=1) with H_2 is even less than for CN(v=0).[1,14] Thus, the presence of CN-(v=1) should not influence the thermal rate constant determination, as argued previously,[3] and likely the intramolecular kinetic isotope effect should be similar for CN(v=0) and CN-(v=1) as well.

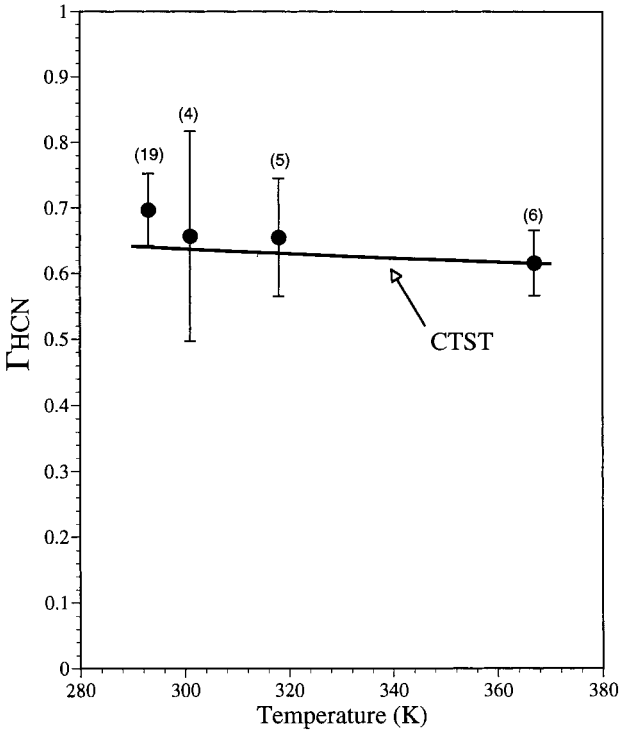

Figure 5. Summary of the determination of the branching ratio, Γ_{HCN}, as a function of temperature. The error bars are the standard deviation in the determination of Γ_{HCN} from the number of measurements indicated in the brackets. The solid curve is the prediction of Γ_{HCN} using the properties of the activated complex from ab initio calculations and CTST.

The calibration factor, cal, was determined under identical experimental conditions as for the determination of Γ_{HCN}, except that H_2 was used instead of HD; however, the vibrational relaxation of CN(v=1) by H_2 is not identical to that by HD. If the vibrational relaxation of CN(v=1) over the short t_{bc}^{CN} delay time were substantially different in the two cases, then the population in the CN(v=0) level would be perturbed and an inappropriate cal value used in the data analysis. There was no evidence for such a process. The CN(v=0) absorbance profiles were well-described by a single-exponential decay rate constant. Furthermore, the most efficient vibrational relaxation partner for CN(v=1) in the system was $(CN)_2$, and at 300 K, Li et al.[39] have measured the vibrational relaxation rate constant at to be 1.1×10^{-13} cm^{3}molecule^{-1} s.$^{-1}$ Estimates of the

TABLE 3: A Summary of the Vibrational Frequencies of the Reactants and Properties of the Transition States for All the Isotopomers for the CN + H_2 Reaction System, at the Same Level of Theory, MR-CI, 3e,3o-CAS+1+2/pvtz Wave Function

			isotopomer			
reactant	vib freq (cm^{-1})	property[a]	H−HCN	D−HCN	H−DCN	D−DCN
CN	2210	ω_{st}	3333	2753	3010	2375
H_2	4393	ω_{st}	2240	2237	2239	2225
HD	3805	ω_{bend}	496	463	398	355
D_2	3107	ω_{bend}	106	95	104	95
		$\omega_{reaction}$	644i	562i	514i	472i
		B	0.7473	0.5491	0.6268	0.4866
		R_{H-H}	0.783			
		R_{H-C}	1.685			
		R_{C-N}	1.156			
		ZPCAE[b]	4.44	4.33	4.54	4.46

[a] Frequency ω in cm^{-1}, B in cm^{-1}, bond lengths R in Å, and zero-point corrected activation energy (ZPCAE) in kcal mol^{-1}. [b] Barrier height 4.2 kcal mol^{-1}.

expected vibrational relaxation rate constants for CN(v=1) relaxation with He or H_2 can be made by a comparison with CO(v=1) relaxation. At 300 K, the vibrational relaxation rate constants for CO by He and H_2 have been measured to be 3×10^{-17} and 3×10^{-16} cm^3 $molecule^{-1}$ $s,^{-1}$ respectively,[40] and relaxation by HD is expected to be of similar magnitude. None of these relaxation processes were sufficiently rapid to perturb the initial CN(v=1)/CN(v=0) population ratio over the short measurement time of t_{bc}^{CN} and, hence, influence the value of the calibration factor, cal.

The rotational energy transfer of CN(v=2;J) has been studied in collisions with both He and Ar and found to be near gas kinetic.[41] The rotational energy transfer for CN(v=0) should be similar, and at a pressure near 4 Torr thermalization was rapid.

The determination of the HCN concentration was made after long delay times, t_{bc}^{HCN}, and the vibrational manifolds of HCN were relaxed, as verified experimentally by monitoring the HCN(001) level in some experiments. Vibrational relaxation rate constants of various HCN levels have been measured by Smith and co-workers[42,43] for He, Ar, and H_2, and the time dependence of several more has been monitored in this laboratory.[17] These measurements show that the HCN vibrational manifold was completely relaxed at the long boxcar delay times used in the present work. The vibrational frequency of HD is in closer resonance with the high-frequency υ_3 mode of HCN than H_2 and should be a more efficient collision partner for vibrational relaxation of HCN than H_2.

IV. Discussion

The results of this work for the determination of the k_{HD} and the Γ_{HCN} as a function of temperature provide new information about the isotope effects in the CN + H_2 system. The new data for the determination of the CN + H_2 and D_2 reaction rate constants obtained in this laboratory[3] were in excellent agreement with measurements by Sun et al.[4] and Sims and Smith[7] over the overlapping temperature ranges. The excellent agreement among several different laboratories using a variety of different techniques over the common temperature region provides strong evidence that the k_{H_2} and the k_{D_2} are well characterized experimentally. Thus, this is an excellent reaction system to compare experimental measurements with theoretical predictions for thermal rate constants and isotope effects as a function of temperature.

There are several possible ways to interpret the isotope effects observed in the CN + H_2 system. One of the simplest is to view the reactivity of each isotopomer as arising from the reactivity of different rotational levels while ignoring any barrier height influence. These arguments can be applied to reactions described by low activation barriers such as F + H_2.[22] The small moment of inertia of the reactants, H_2, D_2, and HD, and the ortho/para nature of H_2 and D_2 results in a large fraction of the reactants in only the first few rotational states even at 300 K; for example, the fraction of the population in $J = 0$ and 1 are 0.13 and 0.67 for H_2, 0.21 and 0.27 for HD, and 0.19 and 0.21 for D_2, respectively. If the reaction cross section has a monotonic dependence on the rotational quantum number of hydrogenic reactant, then it is difficult to rationalize the observed rate constants and branching ratios because of the similar thermal population in the $J = 0$ and 1 levels for HD and D_2. Full-dimensional, quasiclassical trajectory calculations carried out by ter Horst et al.[1] and Bethardy et al.[14] using the TSH3 potential energy surface show that the reaction cross section increases for increasing H_2 rotation. Clearly, the fact that there is a modest potential energy barrier must introduce other considerations in order to explain the observed isotope effects; either zero-point energy effects, tunneling, or saddle point frequency variation on isotopic substitution must play a large role.

A straightforward consideration is to apply CTST to the CN + H_2 reaction system. Wagner and Bair[13] obtained good agreement with the available experimental values for the temperature dependence of k_{H_2} calculated by CTST using the frequencies and structure of the transition state predicted by ab initio theoretical methods. Balla and Pasternack[5] and Sims and Smith[7] used these transition state properties and CTST to extend these calculations to the CN + D_2 system. Sims and Smith found reasonable agreement for the temperature dependence for the rate constants and the kinetic isotope effect. In these cases, the theoretically predicted barrier height was adjusted to obtain agreement with experiment for k_{H_2} at 295 K.

A similar philosophy was adopted in the present work. The transition state properties for CN + H_2 were calculated by ab initio methods, and the properties of all the other transition state isotopomers were calculated by a normal-mode analysis with no adjustments from the theoretical predictions. The transition state for the CN + H_2 reaction was predicted to be linear, and the harmonic frequencies and rotational constants for all the isotopomers are summarized in Table 3. The theoretical calculations have been discussed in detail by ter Horst et al.[1] The transition state properties in Table 3 are based on a MR-CI wave function using a 3e-3o-CAS reference wave function. The calculations employed the Dunning, correlation consistent, polarized triple-ζ (cc-pvtz) basis set. With this level of theory the calculated barrier height was 3.77 kcal mol^{-1}. Note that the highest level of theory reported in ref 1 yielded a predicted, classical barrier height of 4.3 kcal mol^{-1}. The saddle point

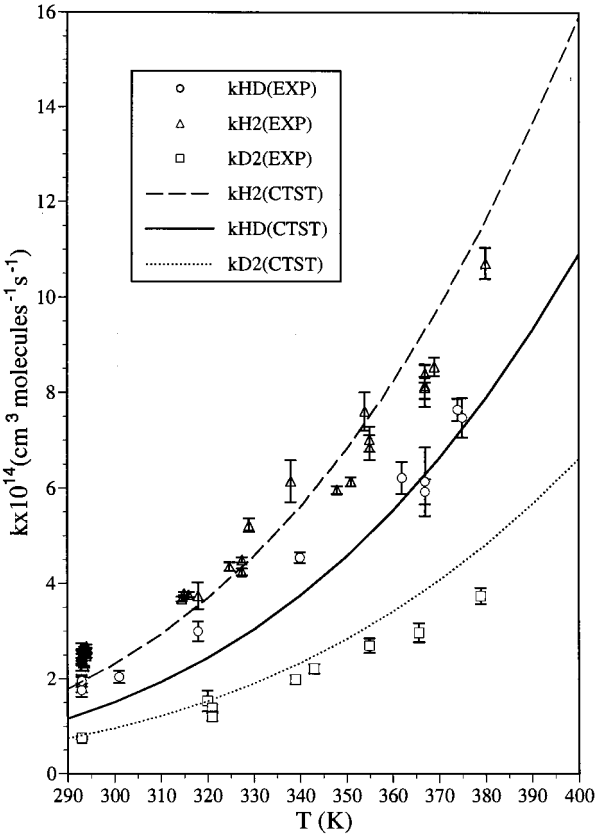

Figure 6. Summary of the determination of the thermal rate constants for CN + H_2, HD, and D_2 measured in this laboratory using time-resolved absorption spectroscopy to follow CN. The lines are the predictions of CTST after the classical barrier height was adjusted to 4.2 kcal mol^{-1} to give agreement with the experimental value of k_{H_2} around 300 K. The error bars are the uncertainty in the least-squares determination of the slopes of plots similar to Figure 3.

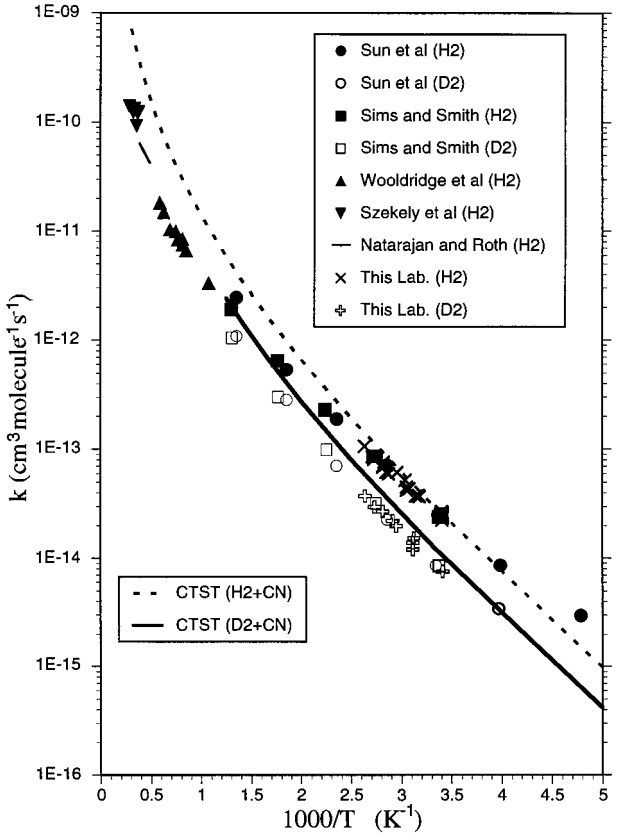

Figure 7. Comparison of selected rate constant data for k_{H_2} and k_{D_2} with CTST calculations based on the saddle point properties derived from ab initio calculations (Table 3) as a function of 1/*T*.

properties in Table 3 are similar to those on the TSH3 surface. The harmonic vibrational frequencies of the reactants, calculated at the same level of theory, are also listed in Table 3. These were used in the CTST calculations in order to obtain a self-consistent zero-point energy corrected barrier height because the transition state frequencies were calculated at the harmonic level only.

The best agreement between the CTST rate constants and the experiment for CN + H_2 over the temperature range 300 K− 400 K was found for a classical barrier height of 4.2 ± 0.1 kcal mol^{-1}. The rate constants for the complete isotopomeric set along with the branching ratio for the CN + HD reaction were calculated as a function of temperature. Quantum mechanical tunneling was accounted for using a Wigner correction.[28] Interestingly, the classical barrier height determined in the CTST calculations was in agreement with the best estimate of the barrier height at the highest level of theory (4.3 kcal mol^{-1}).[1] If the CTST rate constants were calculated using spectroscopic reactant vibrational frequencies, then the CTST calculated classical barrier height would be reduced to 3.9 kcal mol^{-1}.

A comparison of the calculated and experimental rate constants determined in this laboratory, using time-resolved absorption spectroscopy, for the CN + H_2/HD/D_2 systems is shown as a function of temperature in Figure 6, and the calculated branching ratio is included in Figure 5. Over this small temperature range, both theory and experiment are in good agreement for the magnitudes of all the rate constants and the branching ratio.

Usually kinetic isotope effects are dominated by the differences in zero-point energy when the light H atom is substituted for the heavy D atom; however, for the CN + H_2 system this is not the case, and the zero-point corrected activation barriers are quite similar for both the CN + H_2 and CN + D_2 reaction systems, as indicated in Table 3. For these two isotopic pairs the difference in reactivity is largely due to the small rotational partition function of H_2 compared to that of D_2 (almost a factor of 2) and the higher tunneling rate for the light H atom (15% faster at 300 K). On the other hand, for the branching ratio, the CTST rate constants are determined by the properties of the activated complex with the difference between the zero-point corrected activation energies and the influence of tunneling dominating.

It is interesting to extend these calculations to cover a much wider temperature range. Thermal rate constants measurements by Sun et al.[4] and Sims and Smith[7] extend the data for CN + H_2/D_2 from 200 to 800 K, and shock tube experiments by Szelekey et al.,[44] Natarajan and Roth,[45] and Wooldridge et al.[8] provide rate constant data for the CN + H_2 system to over 3500 K. A comparison of the these selected data sets with the CTST calculated rate constants is shown in Figure 7, covering the temperature range 200−3500 K. It is remarkable that this simple theory, using the frequencies and structure of the theoretically calculated transition state, with only a slight adjustment for the barrier height, is in such good agreement with experiment. At 200 K the CTST rate constant for CN + H_2 is a factor of 2 low, and at 3500 K it is a factor of 2 high. The CTST predicted rate constant for the deuterated analogue appears to be in even better agreement with experiment, but over a smaller temperature range.

Che and Liu[10] have measured the excitation function for the CN + D_2 reaction under molecular beam conditions, i.e.,

thermally cold reagents, and found that the reaction cross section started to rise at a collision energy of about 2.5 kcal mol^{-1}, significantly below the zero-point corrected barrier height calculated for the CN + D_2 reaction of 4.46 kcal mol^{-1} (Table 3). At low collision energies, the instrumental resolution was 0.4 kcal mol^{-1} so that these workers suggest that the zero-point corrected barrier height should be around 3.0 kcal mol^{-1}. Tunneling effects would be expected to be small for the heavy D atom. If this barrier height is used to calculate CTST rate constants, then it is necessary to substantially increase the low bending frequencies of the activated complex, to obtain agreement with the thermal rate constant at 300 K. However, this adversely affects the agreement between the calculated and experimental rate constants for the other isotopic combinations. Nevertheless, the tightening up of the transition state frequencies was exactly what was suggested by Wang et al.[12] to obtain better agreement between their new differential cross section measurements and full-dimensional quasiclassical trajectory calculations on the global TSH3 surface. Recently, Manthe and Matzkies used the TSH3 surface to carry out a five-dimensional quantum calculation for k_{H_2} as a function of temperature and found good agreement with experiment.[46] Their results were consistent with a low-frequency bending mode slightly higher ($\sim$150 cm^{-1}) than that defined by a single point on the PES.

It would be highly desirable to have more refined theoretical calculations for the rate constants for the various isotopic combinations in the CN + H_2 system based on the TSH3 surface. The thermal rate constant data for CN + H_2, HD, and D_2 and the wide temperature range over which these data are available provide a solid reliable database in which to compare theoretical predictions and experiment.

Acknowledgment. The authors thank Dr. A. F. Wagner for many stimulating discussions, Dr. J. V. Michael for insight into transition state theory, and Prof. D. Setser for the kind gift of a bottle of cyanogen. This work was supported by the U.S. Department of Energy, Office of Basic Energy Sciences, under Contract W-31-1090-ENG-38.

References and Notes

(1) ter Horst, M. A.; Schatz, G. C.; Harding, L. B. *J. Chem. Phys.* **1996,** *105*, 558.
(2) Yang, D. L.; Lin, M. C. In *The Chemical Dynamics and Kinetics of Small Radicals;* Liu, K., Wagner, A. F., Eds.; World Scientific: Singapore, 1996; Part I, Chapter 5.
(3) He, G.; Tokue, I.; Macdonald, R. G. *J. Phys. Chem. A* **1998**, *102*, 4585.
(4) Sun, Q.; Yang, D. L.; Wang, N. S.; Bowman, J. M.; Lin, M. C. *J. Chem. Phys.* **1990,** *93*, 4730.
(5) Balla, R. J.; Pasternack, L. *J. Phys. Chem.* **1987,** *91*, 73.
(6) Juan, J.; Smith, I. W. M. *J. Phys. Chem.* **1987,** *91*, 69.
(7) Sims, I. R.; Smith, I. W. M. *Chem. Phys. Lett.* **1988,** *149*, 565.
(8) Wooldrige, S. T.; Hanson, R. K.; Bowman, C. T. *Int. J. Chem. Kinet.* **1996**, *28*, 245.
(9) Che, D.-C.; Liu, K. *Chem. Phys. Lett.* **1995,** *243*, 290.
(10) Che, D.-C.; Liu, K. *Chem. Phys.* **1996,** *207*, 367.
(11) Lai, L.-H.; Wang, J.-H.; Che, D.-C.; Liu, K. *J. Chem. Phys.* **1996,** *105*, 3332.
(12) Wang, J.-H.; Liu, K.; Schatz, G. C.; ter Horst, M. *J. Chem. Phys.* **1997,** *107*, 7869.
(13) Wagner, A. F.; Bair, R. A. *Int. J. Chem. Kinet.* **1986,** *18*, 473.
(14) Bethardy, G. A.; Wagner, A. F.; Schatz, G. C.; ter Horst, M. A. *J. Chem. Phys.* **1997**, *106*, 6001.
(15) Takayanagi, T.; Schatz, G. C. *J. Chem. Phys.* **1997**, *106*, 3227.
(16) Coepland, L. R.; Mohammad, F.; Zahedi, M.; Volman, D. V.; Jackson, W. M. *J. Chem. Phys.* **1992**, *96*, 5817.
(17) Bethardy, G. A.; Northrup, F. J.; He, G.; Tokue, I.; Macdonald, R. G. *J. Chem. Phys.*, accepted for publication.
(18) Presser, N.; Gordon, R. J. *J. Chem. Phys.* **1985**, *82*, 1291.
(19) Robie, D. C.; Arepalli, S.; Presser, N.; Kitsopoulos, T.; Gordon, R. J. *Chem. Phys. Lett.* **1987,** *134*, 579.
(20) Zhu, Y.-F.; Arepalli, S.; Gordon, R. J. *J. Chem. Phys.* **1989,** *90*, 183.
(21) Persky, A. *J. Chem. Phys.* **1973**, *59*, 5578.
(22) Johnston, G. W.; Kornweitz, H.; Schechter, I.; Persky, A.; Katz, B.; Bersohn, R.; Levine, R. D. *J. Chem. Phys.* **1991**, *94*, 2749.
(23) Stark. K.; Werner, H.-J. *J. Chem. Phys.* **1996,** *104*, 6515.
(24) Aoiz, F. J.; Banares, L.; Herrero, V. J.; Rabanos, V. S.; Stark, K.; Werner, H.-J. *J. Chem. Phys.* **1995,** *102*, 9248.
(25) Neumark, D. M.; Wodtke, A. M.; Robinson, G. N.; Hayden, C. C.; Lee, Y. T. *J. Chem. Phys.* **1985,** *82*, 3045.
(26) Levine, R. D. *J. Phys. Chem.* **1990**, *94*, 8872.
(27) Talukdar, R. K.; Gierczak, T.; Goldfarb, L.; Rudich, Y.; Rao, B. S. M.; Ravishankara, A. R. *J. Phys. Chem.* **1996,** *100*, 3037.
(28) Johnston, H. S. *Gas-Phase Reaction Rate Theory*; Ronald Press: New York, 1966.
(29) Halpern, J. B.; Huang, Y. *Research in Chemical Kinetics*; Compton, R. G., Hancock, G., Eds.; Elsevier Science: Amsterdam, 1993; Vol. 1.
(30) Bethardy, G. A.; Northrup, F. J.; Macdonald, R. G. *J. Chem. Phys.* **1995**, *102*, 7966.
(31) Smith, I. W. M. In *The Chemical Dynamics and Kinetics of Small Radicals;* Liu, K., Wagner, A. F., Eds.; World Scientific: Singapore, 1996; Part 1, Chapter. 6.
(32) McDaniel, E. W. *Collision Phenomena in Ionized Gases;* John Wiley and Sons: New York, 1964; Chapter 10.
(33) Smith, M. A. H.; Harvey, G. A.; Pellet, G. L.; Goldman, A.; Richardson, D. *J. Mol. Spectrosc.* **1984**, *105*, 105.
(34) Smith, I. W. M. *J. Chem. Soc., Faraday Trans.* 2 **1981**, *77*, 2357.
(35) Knowles, P. J.; Werner, H.-J.; Hay, P. J.; Cartwright, D. C. *J. Chem. Phys.* **1988**, *89*, 7334.
(36) He, G.; Tokue, I.; Macdonald, R. G. *J. Chem. Phys.*, in press.
(37) Press, W. H.; Flannery, B. P.; Teukolsky, S. A.; Vetterling, W. T. *Numerical Recipes: The Art of Scientific Computing*; Cambridge University: Cambridge, 1988.
(38) North, S. W.; Hall, G. E. *J. Chem. Phys.* **1997,** *106*, 60.
(39) Li, X.; Sayah, N.; Jackson, W. M. *J. Chem. Phys.* **1984,** *81*, 833.
(40) Yardley, J. T. *Introduction to Molecular Transfer*; Academic Press: New York, 1980.
(41) Fei, R.; Adelman, D. E.; Carrington, T.; Dugan, C. H.; Filseth, S. V. *Chem. Phys. Lett.* **1995**, *232*, 547.
(42) Cannon, B. D.; Francisco, J. S.; Smith, I. W. M. *Chem. Phys.* **1984**, *89*, 141.
(43) Smith, I. W. M.; Warr, J. F. *J. Chem. Soc., Faraday Trans.* **1991**, *87*, 807.
(44) Szekely, A.; Hanson, R. K.; Bowman, C. T. *Int. J. Chem. Kinet.* **1983**, *15*, 915.
(45) Natarajan, K.; Roth, P. *Proceedings of the 15th Symposium (International) on Combustion*; The Combustion Institute: Pittsburgh, PA, 1988; p 729.
(46) Manthe, U.; Matzkies, F. *Chem. Phys. Lett.* **1998,** *282*, 442.